

Active and Passive IRS Jointly Aided Communication: Deployment Design and Achievable Rate

Min Fu, *Member, IEEE* and Rui Zhang, *Fellow, IEEE*

Abstract—In this letter, we study the wireless point-to-point communication from a transmitter (Tx) to a receiver (Rx), which is jointly aided by an active intelligent reflecting surface (AIRS) and a passive IRS (PIRS). We consider two practical transmission schemes by deploying the two IRSs in different orders, namely, Tx→PIRS→AIRS→Rx (TPAR) and Tx→AIRS→PIRS→Rx (TAPR). Assuming line-of-sight channels, we derive the achievable rates for the two schemes by optimizing the placement of the AIRS with the location of the PIRS fixed. Our analysis shows that when the number of PIRS elements and/or the AIRS amplification power is small, the AIRS should be deployed closer to the Rx in both schemes, and TAPR outperforms TPAR with their respective optimized AIRS/PIRS placement. Simulation results validate our analysis and show the considerable performance gain achieved by the jointly optimized AIRS/PIRS deployment over the existing benchmarks under the same power and IRS element budgets.

Index Terms—Intelligent reflecting surfaces (IRS), active IRS, double IRSs, IRS deployment, rate maximization.

I. INTRODUCTION

Intelligent reflecting surface (IRS) [1] has recently received significant attention from both academia and industry to improve the spectral and energy efficiency of future wireless networks cost-effectively. An IRS typically consists of an array of passive reflecting elements, each of which reflects the incident signal with a desired phase shift and/or amplitude. Unlike conventional active relays, passive IRSs (PIRSs) do not require costly transmit/receive radio-frequency (RF) chains and thus incur significantly lower power consumption [2]. As IRSs can be flexibly deployed in wireless networks to reconfigure wireless channels dynamically, they have been studied for achieving various functions such as coverage extension, rate enhancement, interference mitigation, etc (see, e.g., [1] and the references therein).

Most of the existing works (e.g., [3]–[7]) on IRS have considered the PIRS. Equipped with passive loads (positive resistance), PIRS reflects the incident signal with desired phase shift and reflection gain no larger than one. In addition, PIRSs operate in the full-duplex mode without amplification/processing noise or self-interference [1]. In particular, [3] showed that deploying a single PIRS with N reflecting elements can lead to a squared power scaling order (i.e.,

This work is supported in part by MOE Singapore under Award T2EP50120-0024, National University of Singapore under Research Grant R-261-518-005-720, and The Guangdong Provincial Key Laboratory of Big Data Computing. (*Corresponding author: Rui Zhang.*)

M. Fu is with the Department of Electrical and Computer Engineering, National University of Singapore, Singapore 117583 (e-mail: fumin@nus.edu.sg). R. Zhang is with the Chinese University of Hong Kong, Shenzhen, and Shenzhen Research Institute of Big Data, Shenzhen, China 518172 (e-mail: rzhang@cuhk.edu.cn). He is also with the Department of Electrical and Computer Engineering, National University of Singapore, Singapore 117583 (e-mail: elezhang@nus.edu.sg).

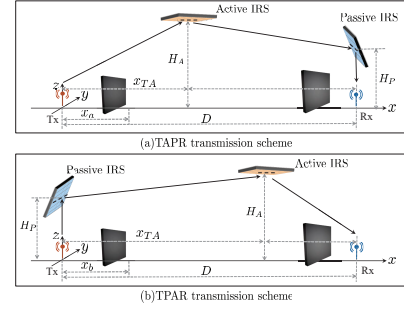


Fig. 1. The illustrations of AIRS-PIRS jointly aided wireless communication. $\mathcal{O}(N^2)$) of the reflected signal, which is even higher than that ($\mathcal{O}(N)$) of the active arrays. Furthermore, [5] proposed a double-PIRS system where N reflecting elements are equally allocated over two distributed PIRSs, which yields an even higher power scaling order ($\mathcal{O}(N^4)$) as compared to the single-PIRS system. Recently, wireless systems aided by multiple PIRSs with multiple signal reflections among them have also been investigated (see [8] and the references therein). Additionally, transmitting passive surfaces were proposed in [9], where they are enclosed on the user's side to allow the incident signal penetration and provide passive beamforming gain for enhancing the performance. Despite the low cost of PIRSs, their signal coverage performance is severely limited by the product-distance path-loss of the cascaded multi-reflection channel [8]. As a result, one PIRS needs to be allocated massive elements and/or deployed near the transmitter (Tx), the receiver (Rx), or other PIRSs in practice to make its signal reflection effective [8].

To address this issue with PIRS, the active IRS (AIRS) has emerged as a promising solution [10]–[15]. With negative resistance components connected to an additional power supply, AIRSs can adjust phase shifts as well as amplitude amplification with a gain exceeding one. Compared to PIRSs, although AIRSs offer an amplification gain (typically lower than that of active relays with dedicated RF amplifiers), they also induce non-negligible amplification noise in their reflected signals [11]. In particular, given the IRS location and the total power budget, an AIRS was shown to achieve higher spectral efficiency [11], energy efficiency [14], and reliability [13] than its PIRS counterpart. Furthermore, with optimized AIRS/PIRS placements, [12] showed that an AIRS only provides a power scaling of $\mathcal{O}(N)$ with N active reflecting elements due to the amplification noise, but it achieves a higher rate than the PIRS when N is small or the AIRS amplification power is high. Nevertheless, the AIRS system design (e.g., AIRS deployment and amplification factor optimization) is more complicated to mitigate noise amplification introduced by the AIRS. Existing research on AIRS has mainly focused on comparing a single

AIRS [10]–[15] or a hybrid IRS comprising active and passive elements [16] to a single PIRS. However, the joint use of distributed AIRS and PIRS in practically challenging scenarios [8] such as multi-turn corridors in an indoor environment has not been studied yet.

To address the above problem, this letter proposes a new wireless communication system jointly aided by a pair of AIRS and PIRS to provide a double-reflection link between a single-antenna Tx and a single-antenna Rx via the two IRSs, while the other links are assumed to be blocked by obstacles. Additionally, we assume that the two IRSs can be properly deployed so that a cascaded line-of-sight (LOS) connection between the Tx and Rx can be established successively through them. Considering two deployment orders for the two IRSs, we present two practical transmission schemes, which are Tx→PIRS→AIRS→Rx (TPAR) and Tx→AIRS→PIRS→Rx (TAPR) schemes, respectively (see Fig. 1). Under the above settings, we aim to characterize the achievable rates for the two schemes with their respective optimized AIRS/PIRS placement. Our analytic results show that for both schemes, when the number of PIRS elements is small, the AIRS should be placed closer to the Rx with decreasing amplification power. Besides, the TAPR scheme generally outperforms the TPAR scheme when the number of PIRS elements and/or the AIRS amplification power is small. Simulation results validate our analysis and demonstrate that the jointly optimized AIRS/PIRS deployment achieves a much higher rate than the existing benchmarks under the same power and IRS element budgets.

II. SYSTEM MODEL AND PROBLEM FORMULATION

As illustrated in Fig. 1, a single-antenna¹ Tx transmits data to a single-antenna Rx² that is D meters (m) away. Under a three-dimensional Cartesian coordinate system, the locations of the Tx and Rx are denoted by $\mathbf{u}_T = (0, 0, 0)$ and $\mathbf{u}_R = (D, 0, 0)$, respectively. A pair of PIRS and AIRS are deployed between them to assist in their communication. The PIRS and AIRS are respectively placed at given altitudes, denoted by H_P and H_A , so that the Tx can communicate with the Rx via only a double-reflection link through the two IRSs over three LOS channels. In particular, we assume that the PIRS is fixed above the Tx or Rx to minimize the path loss, and the AIRS can be flexibly placed between them to maximize the channel gain. Thus, two transmission schemes³ are considered by deploying the PIRS and AIRS in different orders, i.e., TAPR shown in Fig. 1(a) and TPAR shown in Fig. 1(b).

Let N_p and N_a denote the number of passive/active reflecting elements on the PIRS/AIRS, respectively. We further define \mathcal{N}_a and \mathcal{N}_p as the sets containing all the elements on the AIRS and PIRS, respectively. Let $\Theta_P = \text{diag}(\eta_{P,1}e^{j\phi_{P,1}}, \dots, \eta_{P,N_p}e^{j\phi_{P,N_p}})$ and $\Phi_A = \text{diag}(\eta_{A,1}e^{j\phi_{A,1}}, \dots, \eta_{A,N_a}e^{j\phi_{A,N_a}})$ denote the reflection matrices of PIRS and AIRS respectively, where $\eta_{P,n}/\eta_{A,n}$ and $\phi_{P,n}/\phi_{A,n} \in [0, 2\pi)^4$ denote respectively the passive/active re-

flection amplitude and passive/active phase-shift at element n . Therein, for maximal reflection of the PIRS and ease of practical implementation [1], we further set $\eta_{P,n} = 1, \forall n \in \mathcal{N}_p$. Furthermore, since the transmitted signal arriving at all active elements experiences the same path loss under LOS channels, a common amplification factor η should be used to maximize the rate performance as in [11], [14], i.e., $\eta_{A,n} = \eta \geq 1, \forall n \in \mathcal{N}_a$, which also simplifies the design of amplification factors of different IRS elements in practice. Moreover, different from the PIRS that reflects signals without incurring amplification noise, the AIRS generates non-negligible amplification noise at all reflecting elements, which is denoted by $\mathbf{n}_a \in \mathbb{C}^{N_a \times 1}$ and assumed to follow the independent circularly symmetric complex Gaussian distribution, i.e., $\mathbf{n}_a \sim \mathcal{CN}(\mathbf{0}_{N_a}, \sigma_F^2 \mathbf{I}_{N_a})$ with power σ_F^2 .

A. TAPR Transmission Scheme

First, we consider the TAPR scheme with the PIRS fixed above the Rx, as shown in Fig. 1(a).

1) *Signal model*: Denoting the Tx-AIRS horizontal distance as x_{TA} (a design variable), the locations of the PIRS/AIRS are represented by $\mathbf{u}_P = (D, 0, H_P)$ and $\mathbf{u}_A = (x_{TA}, 0, H_A)$, respectively. Thus, the distances between the Rx and PIRS, the Tx and AIRS, and the AIRS and PIRS are respectively given by

$$d_{PR} = H_P, d_{TA}(x_{TA}) = \sqrt{x_{TA}^2 + H_A^2}, \quad (1)$$

$$d_{AP}(x_{TA}) = \sqrt{(D - x_{TA})^2 + (H_P - H_A)^2}. \quad (2)$$

Let $\mathbf{g}_{TA} \in \mathbb{C}^{N_a \times 1}$, $\mathbf{S}_{AP} \in \mathbb{C}^{N_p \times N_a}$, and $\mathbf{h}_{RP}^H \in \mathbb{C}^{1 \times N_p}$ denote the baseband equivalent LOS channels for Tx→AIRS, AIRS→PIRS, and PIRS→Rx links, respectively. Before modeling LOS channels, we first define the one-dimensional steering vector function for a uniform linear array (ULA) as

$$\mathbf{e}(\theta, M') = [1, e^{-j\pi\theta}, \dots, e^{-j\pi(M'-1)\theta}]^T \in \mathbb{C}^{M' \times 1}, \quad (3)$$

where θ denotes the constant phase-shift difference between the signals at two adjacent elements and M' denotes the size of the ULA. For the uniform planar array (UPA) model, each array response vector can be expressed as the Kronecker product of two steering vector functions in the x-axis and y-axis directions, respectively. For example, the array response vector for the UPA from the Tx to AIRS is expressed as

$$\mathbf{a}_{TA}(\theta_{TA}, \vartheta_{TA}, N_a) = \mathbf{e}\left(\frac{2\Delta_A}{\lambda} \sin(\theta_{TA}) \cos(\vartheta_{TA}), N_{a,x}\right) \otimes \mathbf{e}\left(\frac{2\Delta_A}{\lambda} \sin(\theta_{TA}) \sin(\vartheta_{TA}), N_{a,y}\right) \in \mathbb{C}^{N_a \times 1}, \quad (4)$$

where λ denotes the signal wavelength, Δ_A denotes the element space at the AIRS, $(\theta_{TA}, \vartheta_{TA})$ is the angle-of-arrival pair, and $N_{a,x}$ and $N_{a,y}$ denote the number of horizontal/vertical elements at the AIRS with $N_a = N_{a,x} \times N_{a,y}$. As such, \mathbf{S}_{PA} , \mathbf{g}_{AT} , and \mathbf{h}_{PR}^H are respectively given by

$$\mathbf{S}_{AP} = \sqrt{\beta}/d_{AP} e^{-\frac{j2\pi d_{AP}}{\lambda}} \bar{\mathbf{s}}_{AP} \tilde{\mathbf{s}}_{PA}^H, \quad (5)$$

$$\mathbf{g}_{TA} = \sqrt{\beta}/d_{TA} e^{-\frac{j2\pi d_{TA}}{\lambda}} \bar{\mathbf{g}}_{TA}, \mathbf{h}_{RP}^H = \sqrt{\beta}/H_P e^{-\frac{j2\pi H_P}{\lambda}} \bar{\mathbf{h}}_{RP}^H \quad (6)$$

where β denotes the reference channel power at a distance of 1 m, $\bar{\mathbf{s}}_{AP} = \mathbf{a}_{AP}(\theta_{AP}, \vartheta_{AP}, N_p)$, $\tilde{\mathbf{s}}_{PA} = \mathbf{a}_{PA}(\theta_{PA}, \vartheta_{PA}, N_a)$, $\bar{\mathbf{g}}_{TA} = \mathbf{a}_{TA}(\theta_{TA}, \vartheta_{TA}, N_a)$, and $\bar{\mathbf{h}}_{RP} = \mathbf{a}_{RP}(\theta_{RP}, \vartheta_{RP}, N_p)$. In this letter, we assume perfect channel state information (CSI) is available⁵.

⁵The existing channel estimation techniques proposed for double-IRS-aided systems (see e.g., [8]) can be applied to obtain the CSI in our considered system.

¹For the multiple-antenna case, the maximal ratio transmission/combining techniques can be applied at the Tx/Rx.

²This work can be extended to multi-user systems, but the corresponding multi-access design requires further investigation; an initial study on AIRS-aided multiple access is given in [17].

³These two schemes can be practically used for downlink and uplink communications; however, the different deployment order of AIRS and PIRS generally results in different weighted sum-rate performance.

⁴The results in this letter can be extended to the practical setup with discrete phase-shift levels (e.g., by applying the quantization technique [7]).

Though the Tx→AIRS→PIRS→Rx reflecting link, the signal received at the Rx is given by

$$y_a = \mathbf{h}_{\text{RP}}^H \Theta_P \mathbf{S}_{\text{AP}} \eta \Theta_A (g_{\text{TA}} s + \mathbf{n}_a) + e$$

$$= \underbrace{\mathbf{h}_{\text{RP}}^H \Theta_P \mathbf{S}_{\text{AP}} \eta \Theta_A g_{\text{TA}} s}_{\text{Double-reflected signal}} + \underbrace{\mathbf{h}_{\text{RP}}^H \Theta_P \mathbf{S}_{\text{AP}} \eta \Theta_A \mathbf{n}_a}_{\text{Noise introduced by the AIRS}} + e, \quad (7)$$

where s denotes the transmitted signal with power P_t of the Tx, and e denotes the additive white Gaussian noise at the Rx with power σ^2 . As observed from (7), the two IRSs can jointly enhance the double-reflected signal power whereas the AIRS introduces additional amplification noise. The received signal-to-noise ratio (SNR) at the Rx is expressed as

$$\text{SNR}_a(\Theta_A, \Theta_P, \eta, x_{TA}) = \frac{\|\mathbf{h}_{\text{RP}}^H \Theta_P \mathbf{S}_{\text{AP}} \eta \Theta_A g_{\text{TA}}\|^2 P_t}{\|\mathbf{h}_{\text{RP}}^H \Theta_P \mathbf{S}_{\text{AP}} \eta \Theta_A\|^2 \sigma_F^2 + \sigma^2}, \quad (8)$$

and the achievable rate (in bits per second per Hertz or bps/Hz) for the TAPR scheme is given by

$$R_a = \log_2(1 + \text{SNR}_a(\Theta_A, \Theta_P, \eta, x_{TA})). \quad (9)$$

To ensure its reflection amplifier operating in an amplification mode [18] so as to improve the performance over PIRS, the AIRS should be properly deployed to meet the following constraint:

$$\eta \geq 1. \quad (10)$$

Denoting P_F as the given amplification power budget of the AIRS, the amplification power constraint over the signal reflected by the AIRS is given by [11], [12]

$$\eta^2 (P_t \|\Theta_A g_{\text{TA}}\|^2 + \sigma_F^2 \|\Theta_A \mathbf{I}_{N_a}\|^2) \leq P_F. \quad (11)$$

2) *Problem formulation:* We aim to maximize the achievable rate for the Rx by jointly optimizing the reflection matrices at the PIRS/AIRS (i.e., Θ_P and $\eta \Theta_A$) and the AIRS deployment (i.e., x_{TA}). Accordingly, for the TAPR scheme, the optimization problem is formulated as

$$\underset{\substack{\Theta_A, \Theta_P, \eta, \\ x_{TA}}}{\text{maximize}} \quad \log_2(1 + \text{SNR}_a(\Theta_A, \Theta_P, \eta, x_{TA}))$$

$$\text{subject to} \quad |\Theta_P(n, n)| = 1, \forall n \in \mathcal{N}_p, \quad (12a)$$

$$|\Theta_A(n, n)| = 1, \forall n \in \mathcal{N}_a, \quad (12b)$$

$$0 \leq x_{TA} \leq D, \quad (12c)$$

Constraints (10), (11).

Since the objective function is increasing with η , the amplification power constraint in (11) needs to be active at the optimal solution of problem (12). Furthermore, constraint (11) is independent of the phase values in Θ_A and Θ_P . In addition, since the objective function is increasing with $\|\mathbf{h}_{\text{RP}}^H \Theta_P \mathbf{S}_{\text{AP}}\|^2$ and its denominator is independent of the phase value of Θ_A , it is maximized by designing the phases of the AIRS and PIRS to align in the cascaded Tx-AIRS-PIRS-Rx channel. Thus, for given x_{TA} , the optimal phase design of the AIRS/PIRS and amplification factor are respectively given by

$$\Theta_A(n, n) = e^{-j(\angle[\bar{s}_{PA}^H]_n + \angle[g_{\text{TA}}]_n)}, \quad (13)$$

$$\Theta_P(n, n) = e^{-j(\angle[\bar{s}_{AP}]_n + \angle[\mathbf{h}_{\text{RP}}^H]_n)}, \quad (14)$$

$$\eta = \sqrt{P_F d_{TA}^2(x_{TA}) / (P_t N_a \beta + d_{TA}^2(x_{TA}) \sigma_F^2 N_a)}. \quad (15)$$

Combining (13), (14), (15) into (8) yields

$$\text{SNR}_a(x_{TA}) = \frac{P_t P_F \beta^2 N_a N_p^2}{C_1 d_{TA}^2(x_{TA}) + C_2 d_{AP}^2(x_{TA}) + C_3 d_{TA}^2(x_{TA}) d_{AP}^2(x_{TA})}, \quad (16)$$

where $C_1 = \sigma_F^2 P_F \beta N_p^2$, $C_2 = \sigma^2 P_t H_P^2$, and $C_3 = H_P^2 \sigma_F^2 \sigma^2 / \beta$. After substituting (13), (14), and (15) into (12), problem (12) is equivalent to the following,

$$\underset{x_{TA}}{\text{maximize}} \quad \log_2(1 + \text{SNR}_a(x_{TA}))$$

$$\text{subject to} \quad x_a \leq x_{TA} \leq D, \quad (17a)$$

where constraint (17a) corresponds to (10) in problem (12),

$$x_a = \sqrt{\max\{0, N_a \beta P_t / (P_F - N_a \sigma_F^2) - H_A^2\}}. \quad (18)$$

Although the optimal solution to problem (17) is difficult to be characterized in closed form due to the complicated expression of $\text{SNR}_a(x_{TA})$, its value can be obtained by using a one-dimensional search over $x_{TA} \in [x_a, D]$. In the following, we first characterize the effects of AIRS amplification power and the number of PIRS elements on the optimal AIRS placement.

Lemma 1. The optimal Tx-AIRS horizontal distance (i.e., x_{TA}^*) to problem (17) is *non-increasing* with P_F and *monotonically decreasing* with N_p .

Proof. First, it can be shown that x_a in (17a) is non-increasing with P_F . In addition, it is observed that C_1 and $d_{TA}(x_{TA})$ in $\text{SNR}_a(x_{TA})$ monotonically increase with both P_F and x_{TA} while $d_{AP}(x_{TA})$ in $\text{SNR}_a(x_{TA})$ decreases with x_{TA} . As a result, supposing without constraint (17a), when P_F increases, the optimal solution x_{TA}^* should be decreased to guarantee the first derivative of the objective function to be zero. Combining the above, x_{TA}^* is non-increasing with P_F . As for N_p , it can be shown that x_a is independent of N_p while C_1 monotonically increases with N_p . Similarly, it can be concluded that x_{TA}^* is decreasing with N_p . This thus completes the proof. \square

First, as observed from (15), amplification factor η is proportional to x_{TA} and P_F . Based on (8), although the received signal power increases with η and N_p , the AIRS-induced noise is also increased. Thus, from Lemma 1, as P_F and N_p increase, the AIRS has to be deployed closer to the Tx to attenuate the AIRS-PIRS channel gain, thus suppressing its induced noise power at the Rx.

B. TPAR Transmission Scheme

Next, we consider TPAR with the PIRS fixed above the Tx, as shown in Fig. 1(b). Similarly to TAPR, denoting the horizontal distance between the Tx and AIRS as x_{TA} , the locations of the PIRS/AIRS are represented by $\mathbf{u}_P = (0, 0, H_P)$ and $\mathbf{u}_A = (x_{TA}, 0, H_A)$, respectively. The signal model of TPAR is also similar to that of TAPR, while the expressions of the AIRS amplification noise and its power constraint are different since the order of the AIRS/PIRS placements is reversed. The detailed expressions are omitted for brevity.

Similarly to the design of Θ_A and Θ_P in TAPR, the amplification factor and receiver SNR in TPAR are given by

$$\eta = \sqrt{P_F d_{AP}^2 / (P_t N_a \beta^2 N_p^2 / H_P^2 + d_{AP}^2 \sigma_F^2 N_a)}, \quad (19)$$

$$\text{SNR}_b(x_{TA})$$

$$= \frac{N_a \beta^2 N_p^2 P_t P_F}{C_2 / a d_{AP}^2(x_{TA}) + a C_1 d_{AR}^2(x_{TA}) + C_3 d_{AP}^2(x_{TA}) d_{AR}^2(x_{TA})}, \quad (20)$$

where $a = \frac{P_t \sigma^2}{P_F \sigma_F^2}$. As a result, the optimization problem of the TPAR scheme is formulated as

$$\underset{x_{TA}}{\text{maximize}} \quad \log_2(1 + \text{SNR}_b(x_{TA}))$$

$$\text{subject to} \quad x_b \leq x_{TA} \leq D, \quad (21a)$$

where constraint (21a) is due to the amplification power constraint at the AIRS, and

$$x_b = \sqrt{\max\{0, N_a N_p^2 \beta^2 P_t / ((P_F - N_a \sigma_F^2) H_P^2) - (H_P - H_A)^2\}}.$$

Similarly to problem (17), the optimal solution of problem (21) can also be obtained by using the one-dimensional search over $x_{TA} \in [x_b, D]$. Likewise, we have the following lemma for the TPAR scheme.

Lemma 2. The optimal Tx-AIRS horizontal distance (i.e., x_{TA}^*) to problem (21) is *non-increasing* with P_F and *monotonically increasing* with N_p .

Proof. The proof is similar to that of Lemma 1, and thus omitted for brevity. \square

Lemma 2 can be intuitively understood for the TPAR scheme. The AIRS-induced noise is independent of the number of PIRS reflecting elements. As observed from (19), with a smaller P_F and/or a larger N_p , the AIRS should be deployed closer to the Rx to provide a higher amplification factor with $\eta > 1$ and reduce the path loss of the cascaded channel, thus increasing the signal power at the Rx.

III. LOW-COMPLEXITY PLACEMENT DESIGN AND PERFORMANCE COMPARISON

In this section, we present suboptimal AIRS deployment solutions in closed-form for the TAPR and TPAR schemes, respectively. Based on these results, we compare the performance of the two schemes in terms of achievable rate.

A. Suboptimal Solutions

First, to simplify problems (17) and (21), we present a useful lemma as follows (for which the proof is omitted for brevity).

Lemma 3. Given $D \gg \max\{H_A, H_P\}$, we have $C_1 d_{TA}^2(x_{TA}) + C_2 d_{AP}^2(x_{TA}) \gg C_3 d_{TA}^2(x_{TA}) d_{AP}^2(x_{TA})$ and $C_2 / a d_{AP}^2(x_{TA}) + a C_1 d_{AR}^2(x_{TA}) \gg C_3 d_{AP}^2(x_{TA}) d_{AR}^2(x_{TA})$, $\forall x_{TA} \in [0, D]$, if

$$\min\left\{\frac{\sqrt{\beta} N_p \sqrt{P_t \beta}}{H_p \sigma_F} + \frac{\sqrt{P_F \beta}}{\sigma}, \frac{\sqrt{\beta} N_p \sqrt{P_F \beta}}{H_p \sigma} + \frac{\sqrt{P_t \beta}}{\sigma_F}\right\} \gg D. \quad (22)$$

1) *TAPR Scheme:* When condition (22) is satisfied, R_a in problem (17) can be approximated as $\bar{R}_a = \log_2(1 + \overline{\text{SNR}}_a)$, where $\overline{\text{SNR}}_a = \frac{P_t P_F \beta^2 N_a N_p^2}{C_1 x_{TA}^2 + C_2 (D - x_{TA})^2}$. Therefore, problem (17) is approximated as

$$\begin{aligned} & \underset{x_{TA}}{\text{maximize}} \quad \log_2 \left(1 + \frac{P_t P_F \beta^2 N_a N_p^2}{C_1 x_{TA}^2 + C_2 (D - x_{TA})^2} \right) \\ & \text{subject to} \quad \text{constraint (17a)}. \end{aligned} \quad (23)$$

By setting the first derivative of the objective function of (23) with respect to x_{TA} to zero and then projecting it into the feasible set of problem (23), the optimal solution to problem (23) can be obtained as

$$x_{TA}^a = \max\left\{\frac{aD}{a+b}, x_a\right\}, \quad (24)$$

where $a = \frac{P_t \sigma^2}{P_F \sigma_F^2}$ and $b = \frac{\beta N_p^2}{H_P^2}$. Note that when $\frac{aD}{a+b} > x_a$, the amplification factor (i.e., η) in problem (12) is larger than 1. Given $\eta > 1$, the receiver SNR is approximated as

$$\overline{\text{SNR}}_a = \frac{P_F \beta N_a}{D^2 \sigma^2} (a+b) = \frac{\beta N_a}{D^2} \left(\frac{P_t}{\sigma_F^2} + \frac{P_F N_p^2 \beta}{\sigma^2 H_p} \right). \quad (25)$$

2) *TPAR Scheme:* Similarly, based on Lemma 3, problem (21) is approximated as

$$\begin{aligned} & \underset{x_{TA}}{\text{maximize}} \quad \log_2 \left(1 + \frac{P_t P_F \beta^2 N_a N_p^2}{1/a C_2 x_{TA}^2 + a C_1 (D - x_{TA})^2} \right) \\ & \text{subject to} \quad \text{constraint (21a)}. \end{aligned} \quad (26)$$

Similarly to problem (23), the optimal solution to problem (26) is obtained as

$$x_{TA}^b = \max\left\{\frac{abD}{ab+1}, x_b\right\}. \quad (27)$$

Given $\eta > 1$, the approximated receiver SNR is given by

$$\overline{\text{SNR}}_b = \frac{P_F \beta N_a}{D^2 \sigma^2} (ab+1) = \frac{\beta N_a}{D^2} \left(\frac{P_t N_p^2 \beta}{\sigma_F^2 H_p} + \frac{P_F}{\sigma^2} \right). \quad (28)$$

B. Comparisons between TPAR and TAPR

With the suboptimal AIRS deployments given in (24) and (27), the achievable rates for the TPAR and TAPR schemes are compared as follows.

Proposition 1. Given $\eta > 1$ and $N_p \leq \frac{H_P}{\sqrt{\beta}}$, the achievable rate of the TPAR scheme is no less than that of the TAPR scheme, i.e., $\bar{R}_a \geq \bar{R}_b$, if

$$P_F \leq \frac{P_t \sigma^2}{\sigma_F^2}. \quad (29)$$

Otherwise, $\bar{R}_a < \bar{R}_b$. The result is reversed when $N_p \geq \frac{H_P}{\sqrt{\beta}}$.

Proof. Comparing \bar{R}_a and \bar{R}_b is equivalent to comparing $\overline{\text{SNR}}_a$ and $\overline{\text{SNR}}_b$. Thus, with $\eta > 1$, based on (25) and (28), we have

$$\begin{aligned} \overline{\text{SNR}}_a - \overline{\text{SNR}}_b &= \frac{P_F \beta N_a}{D^2 \sigma^2} (a+b-ab-1) \\ &= \frac{\beta N_a}{D^2} \frac{\left(\frac{P_t}{\sigma_F^2} - \frac{P_F}{\sigma^2}\right) (H_P^2 - N_p^2 \beta)}{H_p^2}. \end{aligned} \quad (30)$$

Based on (30), we can conclude that $\bar{R}_a \geq \bar{R}_b$, if

$$N_p \leq \frac{H_P}{\sqrt{\beta}}, \frac{P_F}{\sigma^2} \leq \frac{P_t}{\sigma_F^2}, \text{ or } N_p \geq \frac{H_P}{\sqrt{\beta}}, \frac{P_F}{\sigma^2} \geq \frac{P_t}{\sigma_F^2}. \quad (31)$$

Otherwise, $\bar{R}_a < \bar{R}_b$. This thus completes the proof. \square

IV. NUMERICAL RESULTS

In this section, we present numerical results to compare the rate performance of the TAPR and TPAR schemes in an AIRS-PIRS jointly aided communication system. If not specified otherwise, the simulation parameters are set as follows. The AIRS and PIRS are assumed to be deployed at altitudes of $H_A = 6$ m and $H_P = 5$ m, respectively. The carrier frequency is 3.5 GHz and thus the reference channel gain is $\beta = (\lambda/4\pi)^2 = -43$ dB, with the carrier wavelength $\lambda = 0.087$ m. Other parameters are set as $D = 30$ m, $P_t = 20$ dBm, $\sigma^2 = -80$ dBm, and $\sigma_F^2 = 4\sigma^2 = -74$ dBm. Under our simulation setup, we consider a limited budget of reflecting elements with $N_a < N_p < \frac{H_P}{\sqrt{\beta}} \approx 700$ (see Proposition 1). The numbers of AIRS and PIRS elements are thus fixed as $N_a = 450$ and $N_p = 600$, respectively.

For performance comparison, we consider the existing benchmarks with a single AIRS [12], a hybrid IRS (with active and passive elements) [16], double PIRSs [5], and a single PIRS [7]. For the double-PIRS scheme, both PIRSs are equipped with $(N_a + N_p)/2$ passive elements and deployed above the Tx and Rx, respectively. As for the single-PIRS scheme, the PIRS is equipped with $N_a + N_p$ passive elements and deployed above the Tx or Rx. Furthermore, the transmit power of Tx in the double-PIRS/single-PIRS systems is

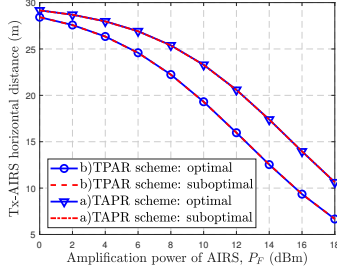


Fig. 2. Optimal AIRS placement versus amplification power of the AIRS.

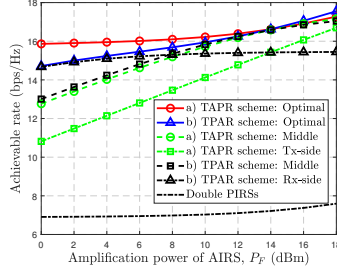


Fig. 3. Achievable rate versus amplification power of the AIRS.

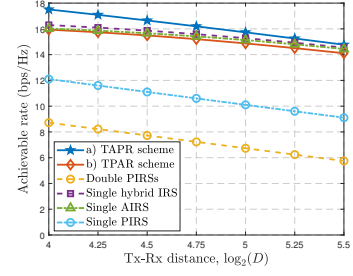


Fig. 4. Achievable rate versus Tx-Rx distance when $P_F = 2$ dBm.

($P_t + P_F$). As such, it is fair to compare it with the AIRS-PIRS jointly aided system. For the latter, we also consider four fixed AIRS/PIRS deployments, where x_{AP} equals $D/2$ or D in both TAPR/TPAR schemes.

Fig. 2 shows the optimal Tx-AIRS horizontal distance versus AIRS amplification power. We observe that the optimal AIRS placement in both schemes is closer to the Rx (i.e., larger x_{TA}) as P_F decreases. This is consistent with Lemmas 1 and 2. Additionally, the proposed suboptimal solution achieves near-optimal performance, validating its effectiveness and the result in Lemma 3.

Fig. 3 compares the achievable rates versus AIRS amplification power. First, as P_F increases, we observe that the rate performance of the AIRS-PIRS jointly aided system increases due to the increasing amplification gain from AIRS. However, compared to these fixed deployment strategies, the AIRS deployment design dynamically balances the signal and noise amplification at the AIRS, thereby further improving performance for both TAPR/TPAR schemes. Furthermore, with the optimal AIRS placement, TAPR performs better than TPAR when $P_F < \frac{P_t \sigma_y^2}{\sigma_F^2}$, because it suffers less path loss of the cascaded channel and thus results in higher received power. These results are consistent with Proposition 1. In addition, thanks to the optimal AIRS/PIRS placement and the resulting amplification gain at AIRS, the AIRS-PIRS jointly aided system achieves a much higher rate than the baseline double-PIRS system under a limited IRS element budget.

Fig. 4 shows that the achievable rate of different schemes with optimal IRS placement versus Tx-Rx distance for $P_F = 2$ dBm. We can observe that TAPR performs better than hybrid-IRS and single-AIRS benchmarks, especially when the Tx-Rx distance is relatively short. This is because TAPR provides higher multiplicative beamforming and amplification gains by jointly using PIRS and AIRS as well as an additional path to attenuate amplification noise as compared to the two single-reflection schemes. This indicates that deploying distributed AIRS and PIRS with the best ordering can be advantageous over combining them into one hybrid IRS or using AIRS only.

V. CONCLUSION

In this letter, we studied a new AIRS-PIRS jointly aided wireless communication system. Under the LOS channel model, we analyzed the effects of the AIRS deployment in two transmission schemes (i.e., TAPR and TPAR) on their achievable rates. Our analysis revealed that the AIRS should be deployed closer to the Rx in both schemes, and TAPR achieves a higher rate than TPAR when the number of PIRS elements and/or AIRS amplification power is limited. Simulation results

validated our analysis and demonstrated that our proposed system considerably outperforms the existing benchmarks in terms of achievable rate, and the performance gain highly depends on the AIRS/PIRS deployment.

REFERENCES

- [1] Q. Wu, S. Zhang, B. Zheng, C. You, and R. Zhang, "Intelligent reflecting surface-aided wireless communications: A tutorial," *IEEE Trans. Commun.*, vol. 69, no. 5, pp. 3313–3351, May 2021.
- [2] D. Renzo *et al.*, "Reconfigurable intelligent surfaces vs. relaying: Differences, similarities, and performance comparison," *IEEE Open J. Commun. Soc.*, vol. 1, pp. 798–807, Jun. 2020.
- [3] Q. Wu and R. Zhang, "Intelligent reflecting surface enhanced wireless network via joint active and passive beamforming," *IEEE Trans. Wireless Commun.*, vol. 18, no. 11, p. 5394–5409, Aug. 2019.
- [4] W. Ma, L. Zhu, and R. Zhang, "Passive beamforming for 3-D coverage in IRS-assisted communications," *IEEE Wireless Commun. Lett.*, vol. 11, no. 8, pp. 1763–1767, Aug. 2022.
- [5] Y. Han, S. Zhang, L. Duan, and R. Zhang, "Double-IRS aided MIMO communication under LoS channels: Capacity maximization and scaling," *IEEE Trans. Commun.*, vol. 70, no. 4, pp. 2820–2837, Apr. 2022.
- [6] B. Zheng, C. You, and R. Zhang, "Double-IRS assisted multi-user MIMO: Cooperative passive beamforming design," *IEEE Trans. Wireless Commun.*, vol. 20, no. 7, pp. 4513–4526, Jul. 2021.
- [7] M. Fu, Y. Zhou, Y. Shi, and K. B. Letaief, "Reconfigurable intelligent surface empowered downlink non-orthogonal multiple access," *IEEE Trans. Commun.*, vol. 69, no. 6, pp. 3802–3817, Jun. 2021.
- [8] W. Mei, B. Zheng, C. You, and R. Zhang, "Intelligent reflecting surface-aided wireless networks: From single-reflection to multireflection design and optimization," *Proc. IEEE*, vol. 110, no. 9, pp. 1380–1400, Sept. 2022.
- [9] K. Liu, Z. Zhang, L. Dai, and L. Hanzo, "Compact user-specific reconfigurable intelligent surfaces for uplink transmission," *IEEE Trans. Commun.*, vol. 70, no. 1, pp. 680–692, Jan. 2022.
- [10] Z. Zhang, L. Dai, X. Chen, C. Liu, F. Yang, R. Schober, and H. V. Poor, "Active RIS vs. passive RIS: Which will prevail in 6G?" *arXiv preprint arXiv:2103.15154*, 2021.
- [11] R. Long, Y.-C. Liang, Y. Pei, and E. G. Larsson, "Active reconfigurable intelligent surface-aided wireless communications," *IEEE Trans. Wireless Commun.*, vol. 20, no. 8, pp. 4962–4975, Aug. 2021.
- [12] C. You and R. Zhang, "Wireless communication aided by intelligent reflecting surface: Active or passive?" *IEEE Wireless Commun. Lett.*, vol. 10, no. 12, pp. 2659–2663, Dec. 2021.
- [13] M. H. Khoshafa, T. M. N. Ngatched, M. H. Ahmed, and A. R. Ndjiongue, "Active reconfigurable intelligent surfaces-aided wireless communication system," *IEEE Commun. Lett.*, vol. 25, no. 11, pp. 3699–3703, Nov. 2021.
- [14] K. Liu, Z. Zhang, L. Dai, S. Xu, and F. Yang, "Active reconfigurable intelligent surface: Fully-connected or sub-connected?" *IEEE Commun. Lett.*, vol. 26, no. 1, pp. 167–171, Jan. 2022.
- [15] K. Zhi, C. Pan, H. Ren, K. K. Chai, and M. Elkashlan, "Active RIS versus passive RIS: Which is superior with the same power budget?" *IEEE Commun. Lett.*, vol. 26, no. 5, pp. 1150–1154, May 2022.
- [16] N. T. Nguyen, Q.-D. Vu, K. Lee, and M. Juntti, "Hybrid relay-reflecting intelligent surface-assisted wireless communications," *IEEE Trans. Veh. Technol.*, vol. 71, no. 6, pp. 6228–6244, Jun. 2022.
- [17] G. Chen, Q. Wu, C. He, W. Chen, J. Tang, and S. Jin, "Active IRS aided multiple access for energy-constrained IoT systems," *IEEE Trans. Wireless Commun.*, 2022, doi: 10.1109/TWC.2022.3206332.
- [18] F. Amato, C. W. Peterson, B. P. Degnan, and G. D. Durgin, "Tunneling RFID tags for long-range and low-power microwave applications," *IEEE J. Radio Freq. Identif.*, vol. 2, no. 2, pp. 93–103, Jun. 2018.